

Copyright 1999, Society of Photo-Optical Instrumentation Engineers

This paper was published in Advances in Resist Technology and Processing XVI, Volume 3678 and is made available as an electronic reprint with permission of SPIE. One print or electronic copy may be made for personal use only. Systematic or multiple reproduction, distribution to multiple locations via electronic or other means, duplication of any material in this paper for a fee or for commercial purposes, or modification of the content of the paper are prohibited.

Optimization of 300 mm coat, exposure, and develop processes for 180 nm and smaller features

Walter H. Swanson^{*a}, John S. Petersen^{*b}, Wang-Pen Mo^{*c&d}, Joseph A. Heck^{*c&e}

^aTokyo Electron America, Inc. 2400 Grove Boulevard Austin, TX 78741-6500

^bPetersen Advanced Lithography, PO Box 162712, Austin, TX 78716 ^cSEMATECH
2706 Montopolis Dr. Austin, TX 78741-6499 ^dAssignee from Taiwan Semiconductor
Manufacturing Company ^eAssignee from Intel

ABSTRACT

To meet the technology needs at their insertion into integrated circuit manufacturing, the testing and development processes of 300 mm wafer compatible tools require imaging of 180 nm and smaller features. In response to this need, processes employing commercially available chemicals intended for use on 200 mm substrates and capable of producing 180 nm and smaller features were developed. Said processes were later used for examining critical dimension control on 300 mm wafers. The methods and the experimental designs used to optimize 300 mm coat, exposure, and develop processes for two positive acting, chemically amplified resist systems are described. A low activation energy resist, PEK-111A3 (Sumitomo Chemical), and a high activation energy resist, UV6 (Shipley Company), were coated on top of DUV42-6 anti-reflection layer (Brewer Science). Results show both resists capable of 140 nm equal line and space processing with process window size limited only by phase errors of the alternating phase-shift mask that induce image placement problems.

Key words: 300 mm wafer, chemically amplified resist, DUV, lithography simulation, alternating phase-shift mask, altPSM, optical proximity correction, OPC, next-generation, lithography, NGL, MEEF, mask error enhancement function

1. INTRODUCTION

Once IC demand requires new manufacturing capacity, the driving force for wafer size conversion will be economical. Indeed, it is expected that the yields from 300 mm wafers will increase by a factor of as much as 2.5X over those realized with 200 mm. In other words, chips produced on 300 mm wafers will be approximately 38 percent less expensive than those manufactured on 200 mm wafers¹. More likely than not, said chips will be produced with optical lithography instead of some next-generation lithography (NGL) technique. Coincidentally, the driving force to manufacture chips containing subwavelength features with optical lithography is economical as well. The costs associated with extending optical lithography are more bearable than NGL costs. This is what DELPHI (DEtermining the Limits of PHotolithography), an International SEMATECH project, concluded². DELPHI suggests that in order to maximize return on investment, the design of the resist system and the exposure tool should be used to simplify reticle design as much as possible. To insure a simplified reticle design, circuit design and layout must be limited to simple geometries so that there are no critical features at angles. DELPHI also suggests that in order to avoid phase conflicts, the use of designs that are alternating phase-shift mask (altPSM) friendly is recommended³.

AltPSM technology improves linewidth control for feature sizes that push the optical resolution limits of a projection system. Although altPSMs are difficult to manufacture and costly, good critical dimension (CD) control can be obtained with them even when the k_1 factor ($k_1 = CD \times NA / \lambda$) is < 0.5 ⁴. Using double-exposure strong PSMs, Hua-Yu Liu *et al.* were successful in printing 140 nm poly gates with a k_1 factor of 0.237. The same authors showed that compared to conventional binary masks, the criticality of mask CD control is reduced for PSMs and that PSMs are less sensitive to mask defects⁵. A strong PSM and 248 nm

*Correspondence: Email: wswanson@aus.telusa.com TEL: (512)424-1391 FAX: (512)424-1039
jpetersen@advlitho.com TEL: (512)327-5817 FAX: (512)327-1510
wang-pen.mo@intl.semtech.org TEL: (512)356-7120 FAX: (512)356-3618
joseph.A.Heck@intel.com

lithography were used to generate the subwavelength features discussed in this paper. The subwavelength features were printed with two positive acting, chemically amplified resist systems that are representative of low and high activation energy (E_A) resists. Low E_A resists contain protecting groups that are extremely reactive to acid. Once exposed, low E_A resists are deprotected by photogenerated acid prior to post-exposure bake (PEB) processing. Consequently, low E_A resist systems are known to have low sensitivity to variations in PEB. High E_A resists, on the other hand, have protecting groups that are less reactive to acid and are therefore, more thermochemically stable. Since high E_A resists use lower-reactivity protecting groups, high-temperature (near or greater than the glass transition temperature) post-application bakes (PABs) and PEBs may be performed. High E_A resist systems require thermal activation for catalytic deprotection of the resin to occur and are less forgiving with respect to variations in PEB⁶.

While several other resist systems would have sufficed, Sumitomo's PEK-111A3, a low E_A resist, and Shipley's UV6, a high E_A resist, were selected. The intent of the authors was not to compare and contrast the resist systems of two photoresist manufacturers but rather, compare and contrast the process performance afforded by varying types of resist design. Preliminary experimentation with PEK-111A3 and UV6 revealed that 180 nm line and space features were easily obtainable and that 120 nm line and space features (1:1 duty cycle) cleared only partially regardless of exposure dose. Consequently, we concentrated our efforts on developing processes capable of producing 160 and 140 nm isolated and dense line and space features (mask designed without 150 nm line and space features). Initial experimentation also showed that isolated to dense feature size bias was large (35 to 50 nm) for both resist systems. In an attempt to garner more performance from our processes, experiments designed to lessen the isolated to dense line size bias were executed. Experiments in which PAB and PEB treatments were altered were conducted using the low E_A resist PEK-111A3. In addition to said experiments, the effect of single vs double PEB processing on the high E_A resist, UV6, was examined. Once experimentation was complete, performance stability of developed processes was evaluated based on statistical analysis of results gathered from passive data collections (PDCs). Finally, while the results for both resists showed that adequate process windows exist for making test wafers, phase error of the altPSM limited the window size because of changes in image placement with changes in focus.

2. EXPERIMENTAL

Process development was performed on 300 mm silicon wafers. Wafer coating, exposing, developing, and analysis was conducted at SEMATECH. Experimental conditions appear in Table 1. Experimental conditions that differ from Table 1 will be noted in parentheses above the table concerned. Three slashes (/ / /) within these tables represents unobtained data. Each 300 mm wafer contained one hundred forty-two exposure fields (field size = 22 X 22 mm). Reticle designed with 60% clear area. Resolution performance was based on comparisons and contrasts of 160 and 140 nm isolated and nested lines. Resolution patterns consisted of 20 lines and spaces at various pitches (1:1 and 1:2). Only the center of the exposure field was measured because the reticle was designed in such a manner that no cross-field data was obtainable. To minimize experimental work, PROLITH/2 (version 6.0.2 from FINLE Technologies, Inc.) simulations were used to verify and predict optimal bottom anti-reflective coating (BARC) thickness, exposure dose, and swing curves for dose-to-clear and CD. Experimental responses were compared with simulations then calibrations to PEK-111A3 and UV6 simulations were performed using an estimated bake plate ramp time derived by plotting $1/E_0$ vs PEB time⁷. Using the generated swing curves as guides, design of experiments (DOEs) were produced by SAS software, JMP. The same software was used to analyze experimental responses. BARC material was diluted (28.0949 g DUV42-6 + 2.4040 g of 0.7 PGME + 0.3 PGMEA) at SEMATECH to produce a 64 nm film after curing. Photoresists were diluted by their respective manufacturers to produce the following post-application bake films: 420 to 530 nm (PEK-111A3) and 330 to 440 nm (UV6) for a final spin speed (FSS) range of 1100 to 1900 rpms. On top of 64 nm coated wafers, a photoresist thickness of 470 nm for PEK-111A3 is an exposure maximum while a thickness of 375 nm for UV6 is an exposure minimum on their respective CD swing curves.

Due to the high cost of 300 mm wafers, cross sectional SEM analysis was performed only once to characterize PEK-111A3 linewidths (PEK-111A3 was plumbed to track prior to UV6). In an effort to abate the isolated to dense feature bias in PEK-111A3, PAB temperature was altered. By adjusting the FSS, a film thickness of 471 nm was maintained (PAB = 95.0 °C: FSS = 1535 rpm, PAB = 110.0 °C: FSS = 1465

rpm). Bake conditions marked as “control” represent supplier recommended conditions. Exposure dose adjustments were performed as needed. A PDC was conducted with thirty-two prime wafers arranged among seventy-two cycling wafers (total: one hundred four wafers). Four prime wafers per lot of thirteen wafers were distributed among eight lots. Wafers were arranged in said manner to allow for lot to lot, across lot, and wafer to wafer CD analysis. CD SEM measurements were limited to 140 nm isolated and dense line features for all PDC experiments. After top-down SEM measurements were complete, wafers were reworked at SEMATECH and then used to gather data again. Wafers were cleaned on a Gasonics Millennia asher with O₂ plasma followed by a post-ash clean (NH₃ + H₂O₂ with a de-ionized water rinse) on a VerTEC Cobra cleaning system with VcS technology. Phase measurements of the altPSM were conducted with an atomic force microscope (AFM). Due to calibration problems, the existence of phase errors for the 1:1 duty cycle at 140 nm and 160 nm could not be confirmed but trench depth data and simulation suggests that there is a ten degree error.

2.1. Characterization of BARC, resist thicknesses, and initial imaging

CD swing amplitude is dependent on substrate reflectivity; the lower the reflectivity the lower the CD variations. In order to minimize CD variations, the manufacturer of DUV42-6 recommended a film of 90 nm. At 90 nm of BARC, reflectivity contour plots as a function of DUV42-6, PEK-111A3, and UV6 thicknesses illustrate that substrate reflectivity may be suppressed to 0 to 0.002, see Figures 1 and 2. We chose to process at a BARC thickness of 64 nm. A BARC film of 64 nm affords a relatively low and constant reflectivity over a 300 nm range of resist thickness for both resists. CD contour plots confirm that there is very little change in CD linewidths at said thickness, see Figures 3 and 4. The resist thickness ranges for a 90 nm BARC film are very narrow (~ 20 nm) in comparison. Furthermore, a thinner BARC film translates into a shorter BARC etch time. Shorter BARC etch times minimize lateral etching which results in less CD loss. Consequently a better transfer of pattern information is realized.

Using the manufacturer’s recommended resist processes, a focus and exposure matrix, a dose-to-clear swing, and a CD swing were collected for each resist system. Optimal conditions for PEK-111A3 showed to be a 470 nm film on a 64 nm film of DUV42-6 with 0.3 partial coherence factor. The exposure maximum for 160 and 140 nm dense line features (1:1 duty cycle) was 450 and 510 J/m² respectively. Top down SEM revealed that there was isolated to dense (iso-dense) line size bias. Iso-dense feature size bias was large 40 ~ 50 nm (160 nm) and 30 ~ 40 nm (140 nm). To examine image quality, resolution, and linewidth control, cross sectional SEM measurements of PEK-111A3 were conducted, see Figures 5 to 8. Photoresist and the underlying BARC must be chemically and optically matched if a robust lithographic process with good CD control is desirable. If acid diffusion from one chemical to the other occurs, flawed resist profiles (footing or undercutting) will result. Indications of footing from either optical or chemical sources and undercutting from photoresist development were not apparent.

While passing through focus from negative to positive, pattern collapse of the first line of the meander pattern (Figure 9) was observed for PEK-111A3 in a very positive regime. The first line printed smaller than the other outer lines and was observed to collapse inward toward the rest of the lines, the other outer lines did not collapse. These data imply that the pattern collapse is due to a combination of lens coma, resist thickness, and development.

Optimal exposure dose conditions for UV6 proved to be a 375 nm film of UV6 on a 64 nm film of DUV42-6 with 0.3 sigma. Unlike PEK-111A3, top down SEM revealed no signs of pattern collapse in UV6 even in a very positive regime of focus. Whether this is due to the chemical makeup of UV6 or due to the thinner film of UV6 (almost 100 nm thinner than PEK-111A3) has not been confirmed. Top down SEM showed that iso-dense line size bias was as large as PEK-111A3 for both feature sizes. Attempts were made to abate iso-dense line size bias by changing resist process from a single PEB to a double PEB process. The rationale behind the two-stage PEB, described by Petersen *et al.*⁸, is the low temperature PEB permits the deprotection reaction to go to completion with minimal acid diffusion into unexposed portions of the resist while the high temperature PEB makes it possible to average out the standing wave. Experimenting with UVIIHS (Shipley Company), tandem bakes were used to moderate diffusion of acid, solvent, and quencher to adjust isolated, dense line size bias.

Table 1. Experimental conditions

Coat/Develop process	TEL Clean Track ACT 12
Substrate	MEMC Si (bare) flatness: 0.18 μm SFQR [*] : 25 X 25 mm ²
Bottom anti-reflective layer	Brewer Science DUV42-6: applied on unprimed Si surfaces, target: 64 nm after cure 3000 rpm dispense for 1.0 s, 1.5 ml @ 23.0 °C
Bottom anti-reflective layer cure	60 s on 100 μm proximity gap @ 205.0 °C
Chill plate before resist coat	60 s on 100 μm proximity gap @ 23.0 °C
Resist	Sumitomo PEK-111A3 and Shipley UV6, post application bake film targets: 471 nm under 1550 rpm and 375 nm under 1500 rpm respectively, dispense 1.5 ml @ 23.0 °C
Optical constants measurement	J. A. Woollam M-88 ex-situ multi-wavelength ellipsometer DUV42-6: n = 1.47, k = 0.41 PEK-111A3: n = 1.79, k = 6.12E-03 UV6: n = 1.77, k = 0.01
Solvent	TOK OK82 (0.8 PGME + 0.2 PGMEA)
Coater module temperature / RH	23.0 °C / 45.0%
Post-application bake	PEK-111A3: 90 s on 100 μm proximity gap @ 90.0 °C UV6: 60 s on 100 μm proximity gap @ 130.0 °C
Film thickness measurement	KLA-Tencor Prometrix UV-1250, 49 sites
Exposure	Canon FPA-3000EX3L stepper: 248 nm, NA = 0.60, 0.50, 0.45, sigma = 0.3, 0.5 magnification: 5X, conventional illumination
Reticle	DuPont alternating phase-shift mask without optical proximity correction features size: 6" x 6" x 0.25" pattern: meander
Post-exposure bake	PEK-111A3: 90 s on 100 μm proximity gap @ 110.0 °C UV6: 90 s on 100 μm proximity gap @ 140.0 °C
Development	TOK NMD-3: no surfactants 2.38% TMAH (0.26N), de-ionized water prewet, 60 s single puddle, H nozzle, 160 ml @ 23.0 °C, de-ionized water rinse 250 ml
Top-down CD measurement	Hitachi S-8C40 SEM magnification: 180,000X
Cross sectional CD measurement	Hitachi 4500 SEM magnification: 100,000X
Atomic force measurement	Digital Instruments 5000 tip: tapping etched silicon probe (TESP)

*Site Flatness least sQuare Range

2.2. Characterization of post-exposure bake process for PEK-111A3 and UV6

The PEB bake plate ramp time was determined and used to calibrate PEB processing time in PROLITH/2 simulations. Both resists were PEB processed between 0 to 90 s and the inverse of the dose-to-clear was plotted against the PEB time, see Figure 10. X intercept (7 s) is good approximation of ramp time or the lag time needed for the wafer to attain intended PEB processing temperature. In order to more accurately match experimental conditions with modeling results, the PEB time input parameter of lithography simulators should be actual time – ramp time for both resists. The flatter curve of PEK-111A3 suggests that this low E_A resist is less sensitive to PEB processing. The low E_A resist intercepts the X-axis at zero suggesting that deprotection has already begun while the high E_A resist required seven seconds.

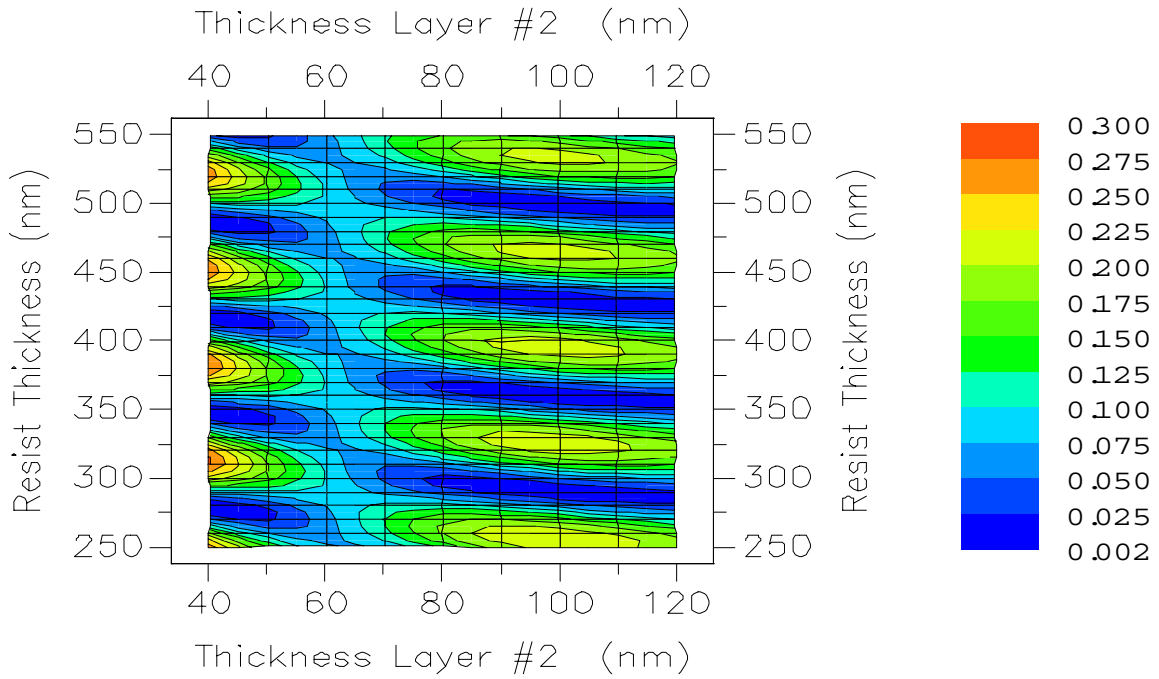


Figure 1. Reflectivity contour plot as a function of DUV42-6 and PEK-111A3 thicknesses. Resist thickness of 470nm on a 64 nm bottom anti-reflective layer has a reflectivity of 0.075 to 0.100 (28.6%).

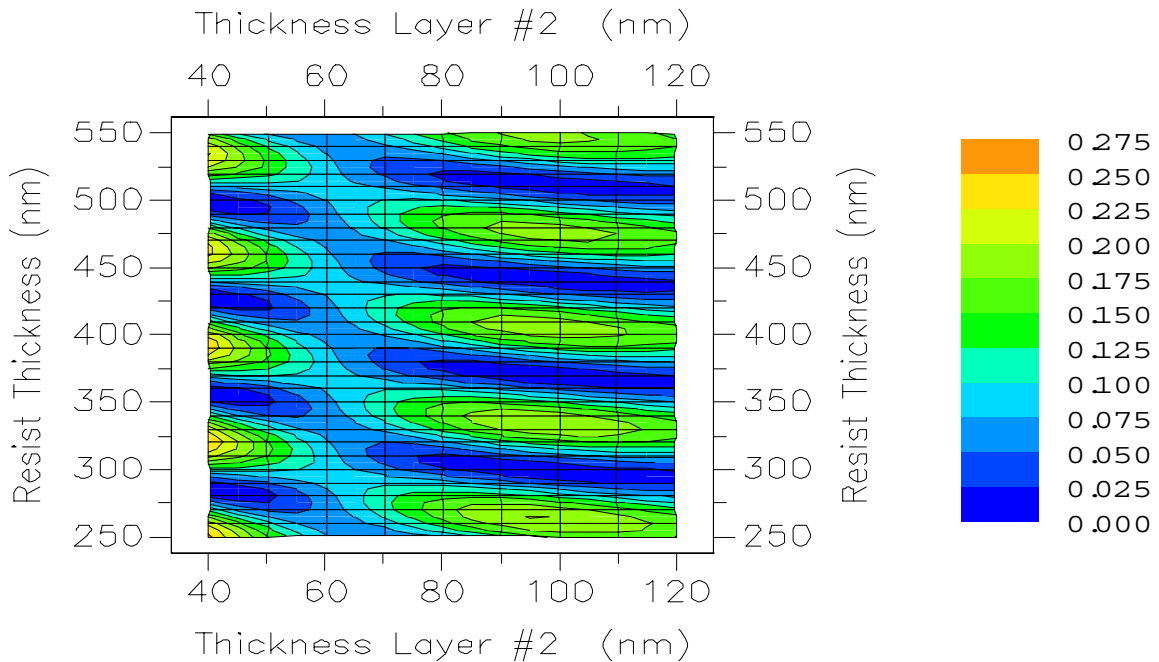


Figure 2. Reflectivity contour plot as a function of DUV42-6 and UV6 thicknesses. Resist thickness of 375 nm on a 64 nm bottom anti-reflective layer has a reflectivity of 0.0500 to 0.075 (40.0%).

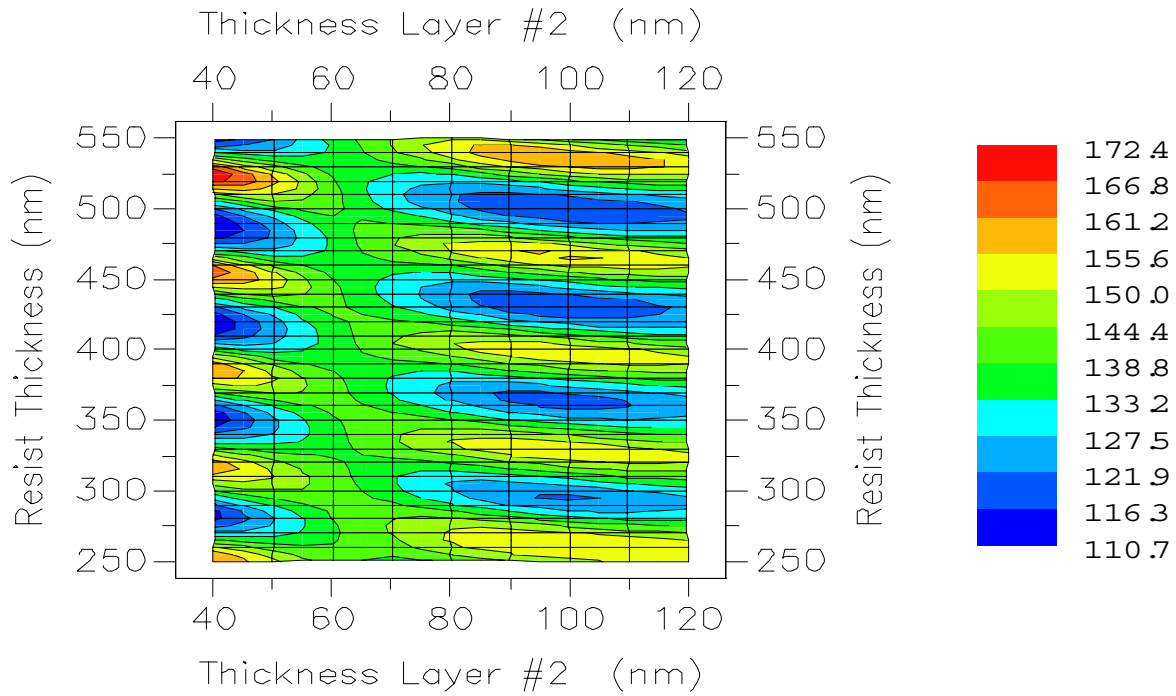


Figure 3. Critical dimension swing contour plot as a function of DUV42-6 and PEK-111A3 thicknesses. Resist thickness of 470 nm on a 64 nm bottom anti-reflective layer has a swing of 133.2 to 138.8 (4.1%).

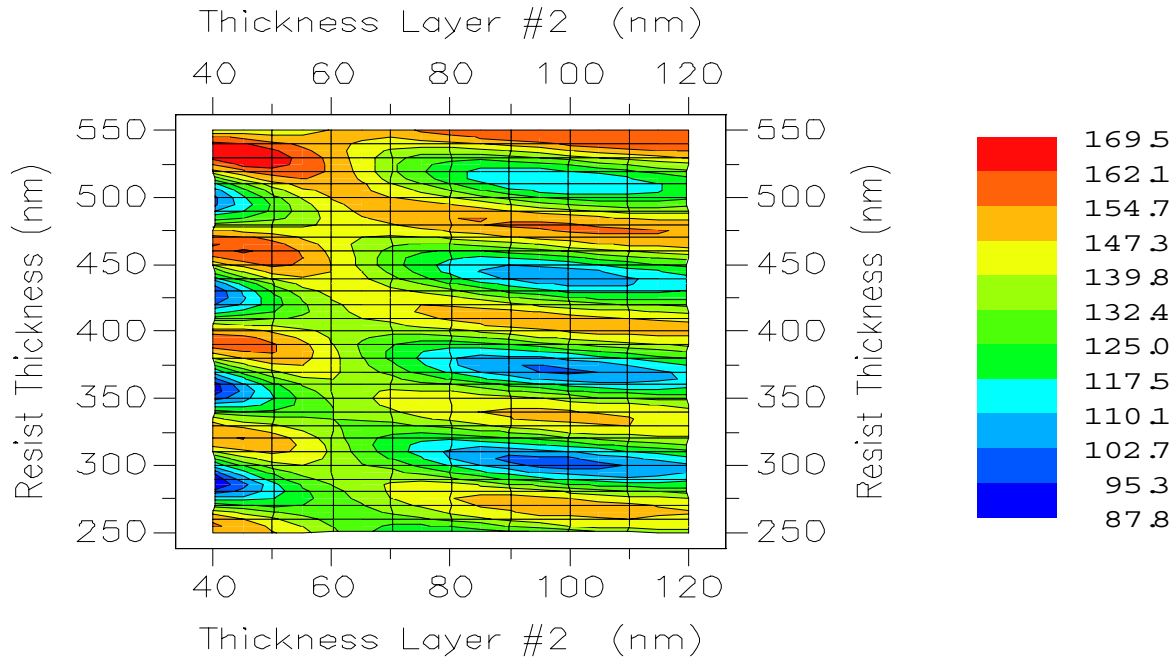


Figure 4. Critical dimension swing contour plot as a function of DUV42-6 and UV6 thicknesses. Resist thickness of 375 nm on a 64 nm bottom anti-reflective layer has a swing of 132.4 ~ 139.8 (5.4%).

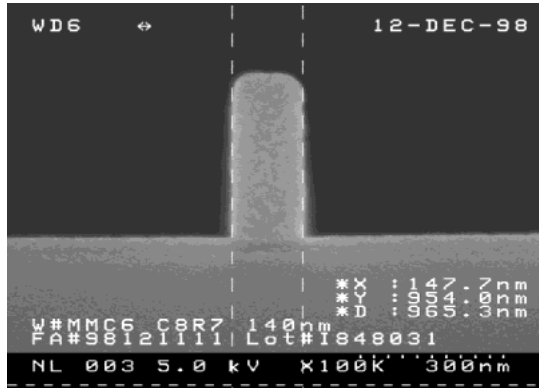


Figure 5. PEK-111A3 140 nm isolated line.

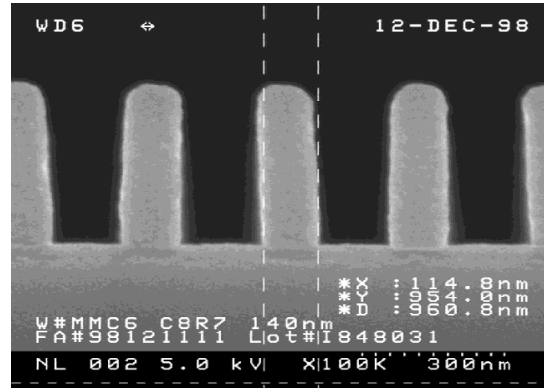


Figure 6. PEK-111A3 140 nm 1:1 dense lines.

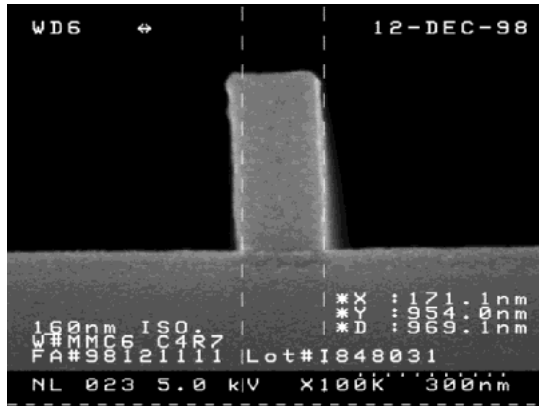


Figure 7. PEK-111A3 160 nm isolated line.

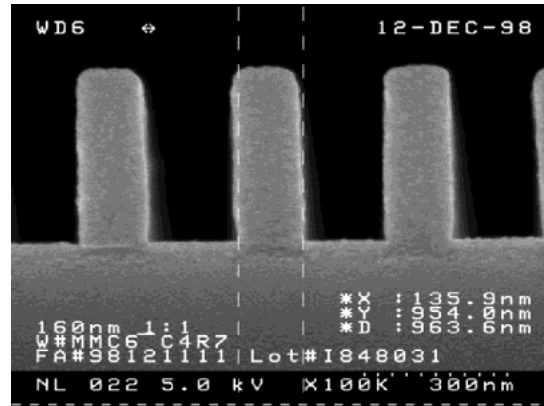


Figure 8. PEK-111A3 160 nm 1:1 dense lines.

2.3. Characterization of the alternating phase-shift mask

The altPSM used for imaging demonstrated a phase error induced image walk with change in focus, see Figure 11. The plate used in these experiments was targeted for 180 nm features. The depth of the 180° trench relative to the 0 trench is targeted for 244 nm for these features and then a portion of the quartz under the chrome is wet etched to try and balance the intensity between shifted and unshifted regions. The data in Table 2 shows that the manufacturer's data achieved the target for the 180 nm features, but that the 120 nm features had a depth of 257 nm. Latter data is consistent with measurements made at International SEMATECH with a Digital AFM. If 244 nm provides a 180° shift then our phase shift used for our imaging is 189° to 194°. A ten degree phase error is consistent with the data shown in Figure 11. This figure shows the change in pitch size relative to focus change and to pitch. Simulation shows that a positive slope is indicative of a positive phase error. The observed image walking reduces the size of the useable process window dramatically for all the features but especially for the 1:1 140 nm.

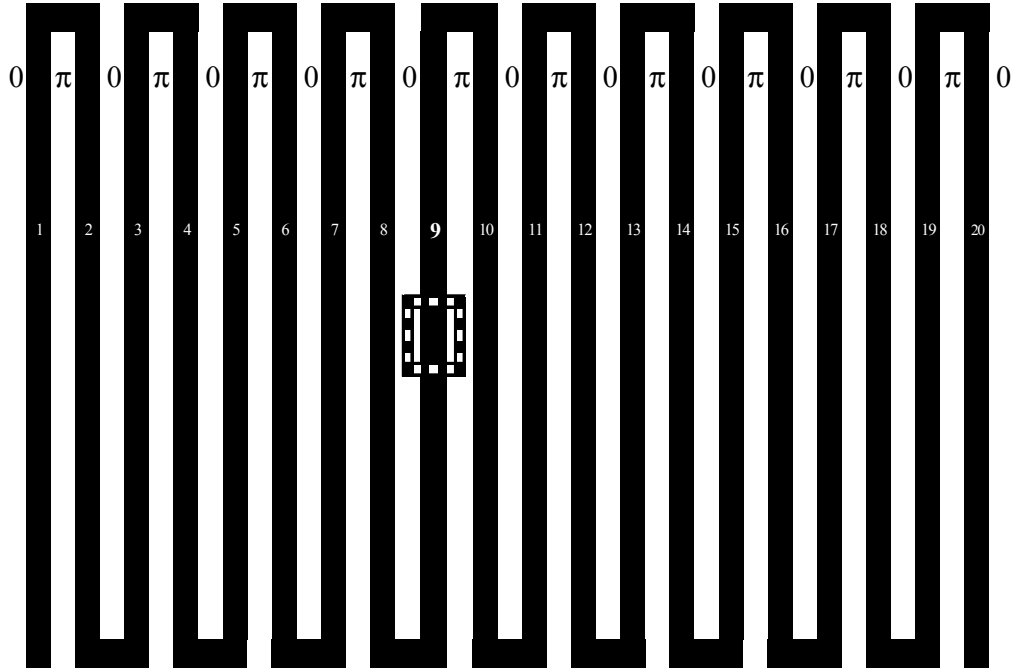


Figure 9. 1:1 dense line/space meander pattern. Center of 9th line is CD measurement location.

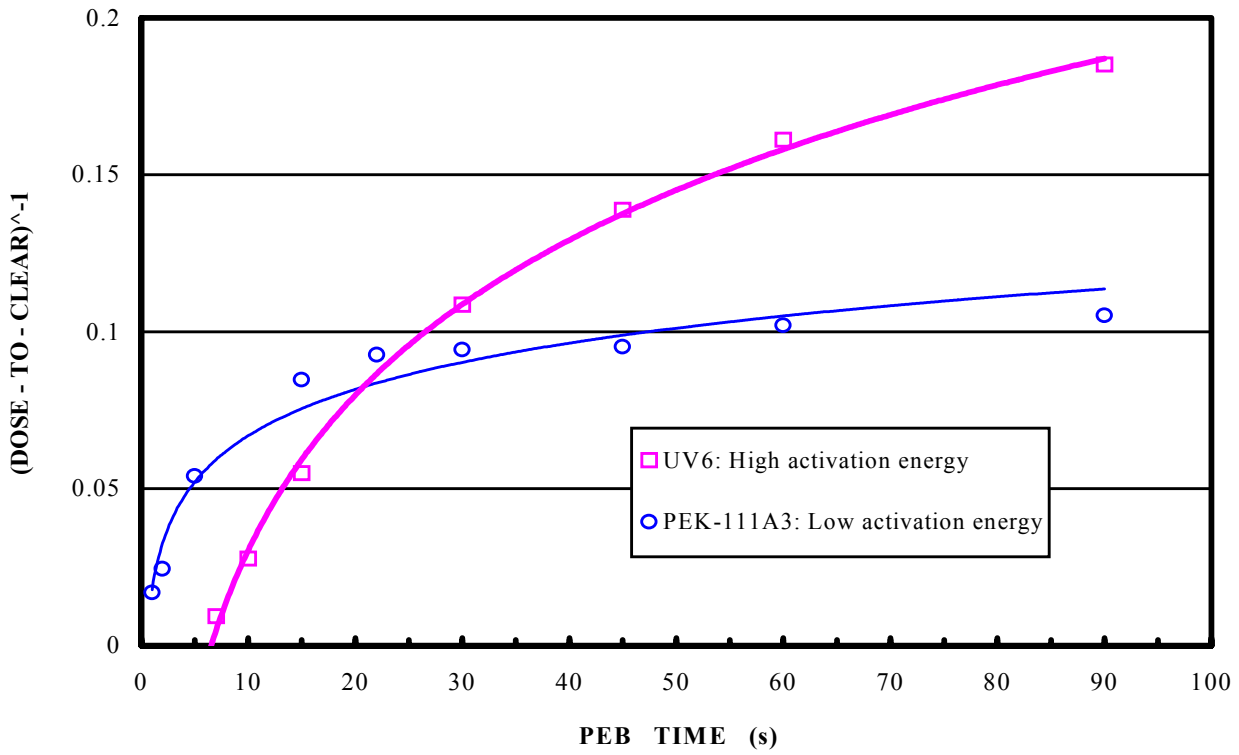


Figure 10. Determining post-exposure bake plate ramp time (X intercept = 7 s) for lithography model tuning.

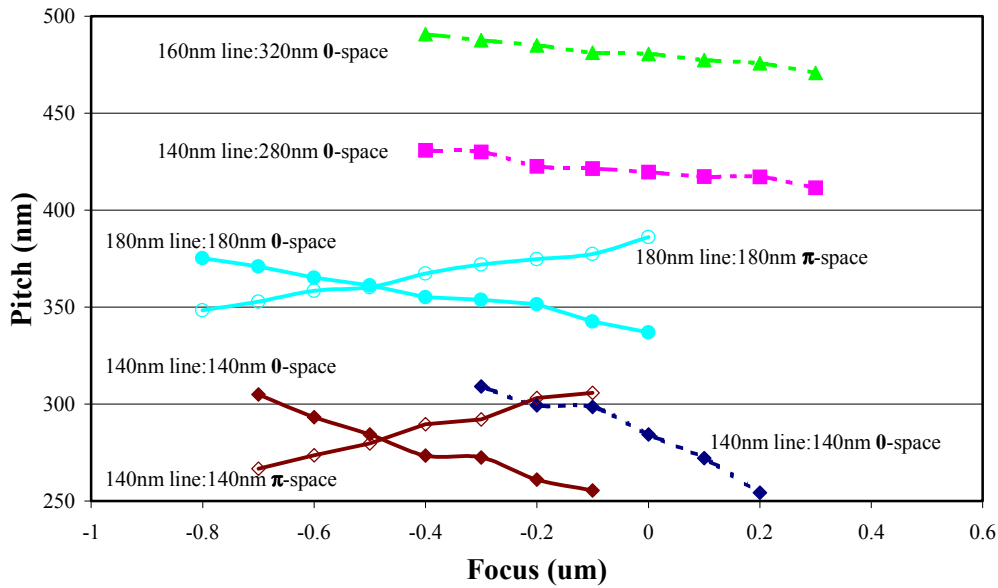


Figure 11. Plot of pitch difference as a linear function through-focus. Solid markers: negative slopes or negative phase errors. Unfilled markers: positive slopes or positive phase errors.

These data are a good example of another component of the mask error enhancement function (MEEF) and suggests that while alternating PSM's CD size variation is cited as a strong reason for choosing the technique over other optical enhancement techniques, phase error can negate its advantages. In this study the depth of focus does not include an image placement constraint but the walking degraded the potential of the process, see Figure 12.

Table 2. Etched quartz depth measurements (IS: International Sematech, DP: DuPont, h: horizontal, v: verticle). **Calculated** Phase values are based on assumption that 180 nm (v), 1 : 2 line : space (244.7 nm) = 180.0 degrees.

Feature Size (nm)	Duty Cycle	Data Org	Measurements (nm)										Calculated			
			1	2	3	4	5	6	7	8	9	10	Avg	Min	Max	Phase
160	1 : 2	IS	258.0	256.3	///	///	///	///	///	///	///	///	257.2	256.3	258.0	189.2
160	Iso	IS	264.3	262.6	///	///	///	///	///	///	///	///	263.5	262.6	264.3	193.8
140	Iso	IS	261.1	260.3	///	///	///	///	///	///	///	///	260.7	260.3	261.1	191.8
180 (h)	1 : 1	DP	244.8	246.3	244.8	246.3	244.8	246.3	244.8	246.3	244.8	246.3	245.6	244.8	244.8	180.6
180 (v)	1 : 2	DP	244.4	244.9	244.4	244.9	244.4	244.9	244.4	244.9	244.4	244.9	244.7	244.4	244.4	180.0
120 (v)	1 : 3	DP	256.6	///	///	///	///	///	///	///	///	///	256.6	256.6	256.6	188.8

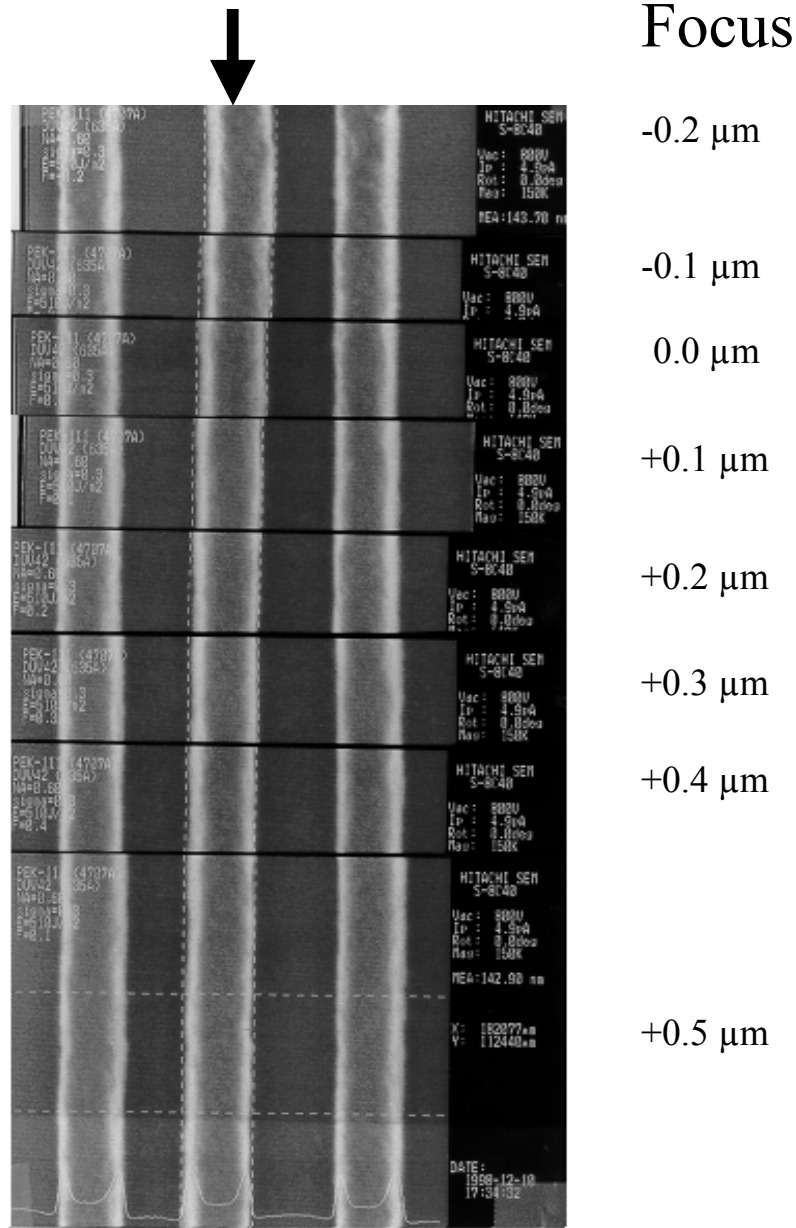


Figure 12. Pitch walking induced by reticle phase error. Profiles are of PEK-111A3 on DUV42-6. 140 nm line/space = 1:1, 0.6NA, 0.3sigma , 510 J/m², 0.3 um. Center line (arrow) is the ninth line of meander pattern.

3. RESULTS AND DISCUSSION

3.1. PEK-111A3 design of experiments

In an effort to reduce line size bias between the two types of features, an experiment in which PAB, PEB temperatures, and the partial coherence factor (sigma) were altered, was performed with PEK-111A3. A report involving another positive acting, chemically amplified resist explains that nested to isolated line bias changed and improved as a result of changes in post-exposure bake⁸. Our results show that increasing the PAB temperature (90.0→110.0 °C) did not influence line size bias but lowering the PEB (120→100.0 °C) and raising the sigma (0.3→0.5) did, see Table 3. Said changes adversely affected depth of focus

Table 3. Experimental design I and results used to determine effect of resist processing conditions on the linewidth process window of PEK-111A3. Underlined **Process Condition** values differ from **Control** values.

Process Condition	Feature Size (nm)	Dense Line			Iso-Dense Bias (nm)
		EL (%)	Eop (J/m ²)	DOF (um)	
Control PAB = 90.0 °C PEB = 110.0 °C Sigma = 0.3	160	~ -6.7/+13.3	450	0.8 (-0.1 ~ 0.7)	~ 45
	140	~ -5.9/+14.7	510	0.7 (-0.1 ~ 0.6)	~ 36
Condition 1 PAB = 90.0 °C PEB = <u>100.0</u> °C Sigma = 0.3	160	~ -8.7/+11.1	460	0.7 (-0.1 ~ 0.6)	~ 41
	140	~ -7.4/+14.8	540	0.6 (0.0 ~ 0.6)	~ 29
Condition 2 PAB = 90.0 °C PEB = <u>100.0</u> °C Sigma = <u>0.5</u>	160	~ -3.6/+7.3	550	0.6 (0.0 ~ 0.6)	~ 12
	140	~ -/+3.2	630	0.1 (0.2 ~ 0.3)	~ 4
Condition 3 PAB = <u>110.0</u> °C PEB = <u>100.0</u> °C Sigma = 0.3	160	~ -/+11.5	520	0.6 (0.0 ~ 0.6)	~ 41
	140	~ -/+10.3	560	0.5 (0.1 ~ 0.6)	~ 35
Condition 4 PAB = <u>110.0</u> °C PEB = <u>100.0</u> °C Sigma = <u>0.5</u>	160	~ -/+9.8	610	0.3 (0.1 ~ 0.4)	~ 23
	140	///	///	///	///
Condition 5 PAB = 90.0 °C PEB = <u>120.0</u> °C Sigma = 0.3	160	~ -/+12.0	500	0.6 (-0.1 ~ 0.5)	~ 48
	140	~ -7.4/+14.8	540	0.5 (-0.1 ~ 0.4)	~ 40
Condition 6 PAB = 90.0 °C PEB = <u>120.0</u> °C Sigma = <u>0.5</u>	160	~ -/+6.9	580	0.6 (-0.1 ~ 0.5)	~ 34
	140	~ -/+3.1	660	0.3 (0.0 ~ 0.3)	~ 14
Condition 7 PAB = <u>110.0</u> °C PEB = <u>120.0</u> °C Sigma = 0.3	160	~ -7.7/+15.4	520	0.7 (-0.1 ~ 0.6)	~ 47
	140	~ -/+10.3	580	0.5 (-0.1 ~ 0.4)	~ 46
Condition 8 PAB = <u>110.0</u> °C PEB = <u>120.0</u> °C Sigma = <u>0.5</u>	160	~ -/+6.7	600	0.7 (-0.1 ~ 0.6)	~ 36
	140	~ -3.0/+0	660	0.5 (-0.1 ~ 0.4)	~ 10

Table 4. Experimental design II and results used to determine effect of post-application and post-exposure baking temperature on the 140 nm linewidth process window of PEK-111A3. Underlined **Bake Condition** values differ from **Control** values.

Bake Condition	Dense Line			Iso-Dense Bias (nm)
	EL (%)	Eop (J/m²)	DOF (um)	
Control PAB = 90.0 °C PEB = 110.0 °C	///	490	~ 0.4	~ 39
Condition 1 PAB = <u>95.0</u> °C PEB = 110.0 °C	///	500	~ 0.4	~ 35
Condition 2 PAB = <u>95.0</u> °C PEB = <u>100.0</u> °C	///	500	~ 0.5	~ 42
Condition 3 PAB = <u>110.0</u> °C PEB = 110.0 °C	///	520	~ 0.5	~ 43
Condition 4 PAB = <u>110.0</u> °C PEB = <u>100.0</u> °C	///	520	~ 0.5	~ 39

Table 5. Experimental design III and results used to determine effect of puddle conditions on 140 nm linewidth process window of PEK-111A3 (PAB = 110.0 °C, PEB = 100.0 °C).

Puddle Condition	Dense Line			Iso-Dense Bias (nm)
	EL (%)	Eop (J/m²)	DOF (um)	
Control Puddle = 60 s	~ +/- 7.1	540	~ 0.5	~ 37
Condition 1 Puddle = 45 s	~ +/- 10.3	580	~ 0.5	~ 30
Condition 2 Puddle = 30 s	~ +/- 8.0	620	~ 0.4	~ 31
Condition 3 Puddle = 45 s agit	~ +/- 10.3	560	~ 0.5	~ 32

The second and third PEK-111A3 DOE were performed one after the other (i.e. DOE II results were not analyzed prior to conducting DOE III), see Tables 4 and 5. Unfortunately, no drastic improvements in iso-dense line size bias was realized by altering PAB and PEB temperatures. Although slight reductions in iso-dense line size bias were obtained by altering developer puddle conditions, reductions were within the noise of the CD SEM repeatability tolerances. Based on top down SEM analysis, a 60 s puddle with agitation (not shown) had the best image.

3.2. UV6 design of experiments

To improve grouped to isolated line size bias in UV6, another approach involving a two step PEB was considered. A two step or double PEB treatment has been shown to improve the lithographic performance of a chemically amplified resist via formation of acid diffusion wells⁸. Petersen *et al.* used a low temperature PEB to permit deprotection reaction to go to completion with minimal acid diffusion. Subsequently, standing waves were averaged out by performing the second PEB process at a high temperature. Since a sigma of 0.5 successfully printed 160 nm and not 140 nm features in PEK-111A3, data was collected using a partial coherence factor of 0.3 (0.4 sigma size aperture was not available). Alteration of UV6 resist processes did not dramatically reduce iso-dense print bias, see Table 6.

Table 6. Experimental design IV and results of UV6 double PEB screening experiment.

Pattern	First PEB	High PEB Time (s)	Low PEB Time (s)	High PEB Temp (°C)	Low PEB Temp (°C)	EL (%)	Eop (J/m ²)	DOF (um)	Iso-Dense Bias
----+	Low	10	50	130	130	~ +/- 7	320	~ 0.6	~ 35
---+-	Low	10	50	140	125	~ +/- 6	370	~ 0.5	~ 34
--+--	Low	10	80	130	125	~ +/- 7	340	~ 0.6	~ 24
--+++	Low	10	80	140	130	~ +/- 7	280	~ 0.6	~ 37
-+---	Low	40	50	130	125	~ +/- 8.5	310	~ 0.6	~ 30
-+-++	Low	40	50	140	130	~ +/- 8	230	~ 0.6	~ 36
-++-+	Low	40	80	130	130	~ +/- 6.5	260	~ 0.5	~ 37
-++++	Low	40	80	140	125	///	///	///	///
+----	High	10	50	130	125	///	///	///	///
+---+	High	10	50	140	130	~ +/- 6	330	~ 0.5	~ 28
+--++	High	10	80	130	130	~ +/- 5	290	~ 0.5	~ 36
+ - + + -	High	10	80	140	125	///	///	///	///
++--+	High	40	50	130	130	~ +/- 7	290	~ 0.5	~ 37
++-+-	High	40	50	140	125	///	220	///	///
++++-	High	40	80	130	125	~ +/- 6	290	~ 0.6	~ 39
+++++	High	40	80	140	130	~ +/- 7	220	~ 0.6	~ 30
Single bake	///	90	///	140	///	~ +/- 7	200	~ 0.5	~ 36
Single bake	///	90	///	130	///	~ +/- 7	280	~ 0.5	~ 36
Single bake	///	///	90	///	130	~ +/- 7	290	~ 0.5	~ 36

The effects of numerical aperture (NA) on iso-dense print bias was examined, see Table 7. Results show that iso-dense line size bias decreases with larger NA (at similar k_{pitch}).

Table 7. UV6 lithographic performance at similar k_{pitch} and different NA (bold values are experimental conditions).

Feature Size (nm)	Dense Duty Cycle	k_{pitch} at 0.45 NA	k_{pitch} at 0.50 NA	k_{pitch} at 0.60 NA	EL (%)	Eop (J/m^2)	DOF (μm)	Iso-Dense Bias
140	1:1	0.508	0.564	0.677	~ +/- 8	340	~ 0.6	~ 31
140	1:2	0.762	0.846	1.016	~ +/- 8	340	~ 0.5	~ 42
160	1:2	0.870	X	X	~ +/- 8	350	~ 0.7	~ 56

3.3. Passive data collection

In order to demonstrate the performance stability of the developed processes, a PDC was conducted. Thirty-two monitor wafers were arranged among seventy-two cycling wafers (total: one hundred four) according to the order shown in Table 8. Data collected from PDCs was used to identify input factors which affect process output.

Table 8. Passive data collection wafer assignment for 32/104 wafers.

Cassette No. 1		Cassette No. 2		Cassette No. 3		Cassette No. 4		Cassette No. 5		Cassette No. 6		Cassette No. 7		Cassette No. 8	
Slot	Order	Slot	Order	Slot	Order	Slot	Order	Slot	Order	Slot	Order	Slot	Order	Slot	Order
1	1	2	15	2	28	4	43	6	58	3	68	2	80	3	94
2	2	4	17	8	34	5	44	9	61	6	71	9	87	6	97
5	5	10	23	9	35	9	48	10	62	9	74	10	88	7	98
9	9	13	26	10	36	11	50	13	65	13	78	12	90	13	104

3.3.1. PEK-111A3 passive data collection

Table 9 shows that lot to lot and wafer to wafer CD variance was significant for the 140 nm isolated lines and that only wafer to wafer CD variance was significant for the dense lines. The CD mean control charts for PEK-111A3 show that the CD mean rises for wafers 1 to 5 and then control is maintained until the seventeenth wafer, see Figure 13. After the seventeenth wafer, the mean falls in and out of control. The loss of control is statistically significant but from an engineering standpoint, the loss of control is acceptable because the isolated CD data remained within +/- 10% nominal. Dense line CD means went out of control only once during the PDC at wafer 15, see Figure 14. Like the 140 nm isolated lines, the 140 nm dense lines displayed good CD control for engineering purposes. Over half of the isolated line CD variance can be accounted for by residual factors (across wafer, systematic, etc. CD variance) while residual factors accounted for almost 93% of dense line variance, see Table 10.

3.3.2. UV6 single PEB passive data collection

The thermal sensitivity of UV6 for isolated/dense features is 5.7/2.6 nm per degree celcius⁹. Our results show that UV6 isolated CD linewidths have a wider distribution than dense. Nominal +/- 10% linewidth control was displayed by UV6 throughout the PDC. Neither lot to lot nor wafer to wafer variance was a significant contributor toward the 140 nm iso-dense line CD linewidth variance, see Table 11. Except for the first wafer, CD control for UV6 140 nm iso-dense line features was maintained throughout the PDC, see Figures 12 and 13. Table 12 shows that almost all the variance for isolated (>96%) and dense (>99%) CD linewidths is attributable to residual factors.

3.3.3. UV6 double PEB passive data collection

Table 13. shows that lot to lot and wafer to wafer variance were not contributing factors in the 140 nm iso-dense CD linewidth variance. The CD mean for the UV6 isolated lines went out of control on wafer 29 while the dense lines fell out of control on wafers 11 and 30, see Figures 17 and 18. Unlike the single PEB process, wafer to wafer variance accounted for over a third of the 140 nm isolated line CD variance while residual factors contributed slightly more than half, see Table 14. Dense line CD variance was due to almost entirely residual factors.

3.3.4. Passive data collection CD contour plots

Seventeen of the one hundred forty-two exposure fields were measured for CD SEM linewidth analysis, see Figure 19. The 140 nm isolated line CD contour plot for PEK-111A3 shows a gradient signature with the center CD linewidths smaller than those near the edge, see Figure 20 (a). Dense lines also display a gradient but the center CD linewidths are larger than those along the edge, see 18 (b). High E_A resists like UV6 are very sensitive to PEB processing. So sensitive in fact, high E_A resist are good indicators of hot plate thermal uniformity¹⁰. For both PEB processes, the 140 nm iso-dense line CD linewidths for UV6 have a gradient signature in which the center CD linewidths are smaller than the CD linewidths close to the edge, see Figures 21 (a, b) and 22 (a, b). Said gradient concurs with data obtained using a SensArray thermocouple attached wafer.

3.3.5. UV6 single PEB vs double PEB passive data collection

Even though the rate of acid diffusion varies greatly between the single and double PEB processes, UV6 demonstrated good CD control for both types of PEB processing. The 140 nm isolated lines for both types of PEB processing have overlapping distributions with slightly different means, see Figure 21. The double and single bake 140 nm dense line CD mean distributions are also slightly different and skewed in opposite directions, see Figure 22. Regardless of PEB processing, variation for the iso-dense line features was ~ 5 nm, see Table 15. Results indicate that UV6 is very insensitive to acid diffusion.

Table 9. PEK-111A3 140 nm iso-dense line CD data analysis of variance (0.6NA, 0.3 σ , 510 J/m², 0.3 μ m, puddle = 60 s w/ agitation).

Component	Degree of Freedom		Sum of Squares		Mean Square		F Ratio		P-Value	
	Iso	Dense	Iso	Dense	Iso	Dense	Iso	Dense	Iso	Dense
Lot	7	7	0.00198	0.00021	0.00028	0.00003	12.0328	2.0258	<0.0001	0.0954
Wafer[Lot]	24	23	0.00057	0.00034	0.00002	0.00001	4.1174	1.9146	<0.0001	0.0067
Error	512	512	0.00293	0.004	6E-06	8E-06	NA	NA	NA	NA
Total	543	542	0.00548	0.00456	1E-05	8.4E-06	NA	NA	NA	NA

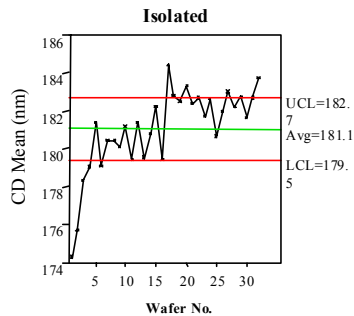


Figure 12. CD mean control charts for 140 nm isolated features.

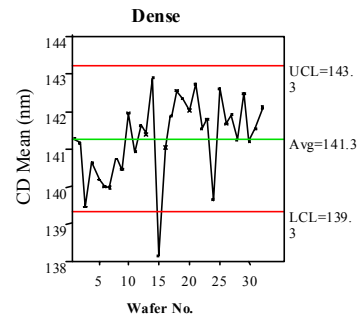


Figure 13. CD mean control charts for 140 nm dense lines for PEK-111A3

Table 10. PEK-111A3 140 nm isolated and dense line variance component estimates (VCE).

Component	Variance Component Estimates		Percent (%) VCE	
	Isolated	Dense	Isolated	Dense
Lot	1.00E-06	2.30E-07	9.09	2.66
Wafer[Lot]	4.00E-06	4.13E-07	36.36	4.78
Residual	6.00E-06	8.00E-06	54.55	92.57
Total	1.10E-05	8.64E-06	100.00	100.00

Table 11. UV6 140 nm iso-dense line CD data analysis of variance for single PEB (0.6NA, 0.3σ 2.00 J/m², 0.1 um)

Component	Degree of Freedom		Sum of Squares		Mean Square		F Ratio		P-Value	
	Iso	Dense	Iso	Dense	Iso	Dense	Iso	Dense	Iso	Dense
Lot	7	7	0.0004	0.0024	0.00006	0.00003	1.3629	1.6252	0.2717	0.183
Wafer[Lot]	21	21	0.00088	0.00044	0.00004	0.00002	1.5173	0.8026	0.0667	0.7176
Error	461	464	0.01271	0.01207	2.8E-05	2.6E-05	NA	NA	NA	NA
Total	489	492	0.014	0.01275	2.9E-05	2.6E-05	NA	NA	NA	NA

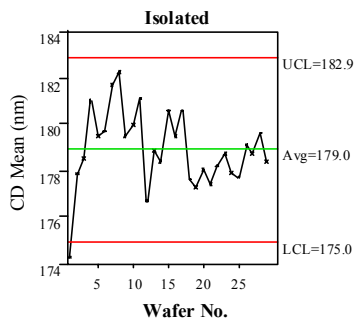


Figure 14. CD mean control charts for 140 nm isolated features

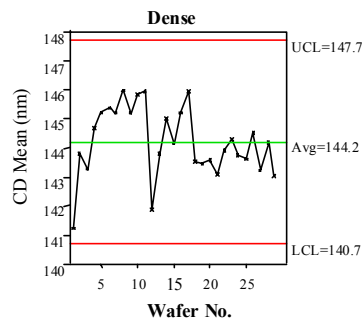


Figure 15. CD mean control charts for 140 nm dense features.

Table 12. UV6 140 nm isolated and dense line variance component estimates (VCE).

Component	Variance Component Estimates		Percent (%) VCE	
	Isolated	Dense	Isolated	Dense
Lot	2.51E-07	2.14E-07	0.86	0.82
Wafer[Lot]	8.44E-07	0.00E+00	2.90	0.00
Residual	2.80E-05	2.60E-05	96.24	99.18
Total	2.91E-05	2.62E-05	100.00	100.00

Table 13. UV6 140 nm iso-dense line CD data analysis of variance for double PEB (0.6NA, 0.3 σ , 3.40 J/m², 0.1 μ m, low PEB = 125°C for 80 s, high PEB = 130°C for 10 s).

Component	Degree of Freedom		Sum of Squares		Mean Square		F Ratio		P-Value	
	Iso	Dense	Iso	Dense	Iso	Dense	Iso	Dense	Iso	Dense
Lot	7	7	0.0004	0.0004	0.00006	0.00003	1.3629	1.3629	0.2717	0.2717
Wafer[Lot]	21	23	0.00088	0.00088	0.00004	0.00001	1.5173	1.5173	0.0667	0.0667
Error	461	512	0.01271	0.01271	2.8E-05	8E-06	NA	NA	NA	NA
Total	489	542	0.014	0.014	2.9E-05	2.6E-05	NA	NA	NA	NA

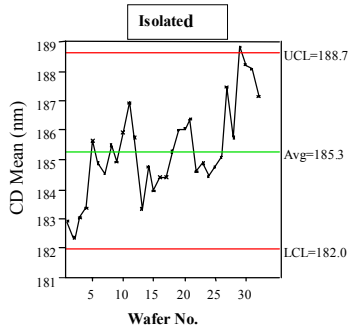


Figure 16. CD mean control charts for 140nm features for double PEB

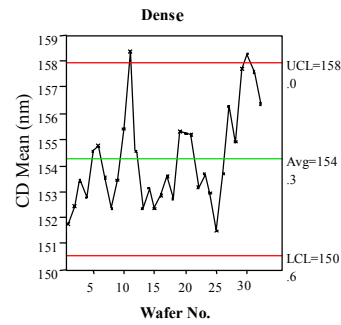


Figure 17. CD mean control charts for 140nm features for double PEB

Table 14. UV6 140 nm iso-dense line variance component estimates (VCE).

Component	Var Comp Est		Percent VCE	
	Iso	Dense	Iso	Dense
Lot	1.00E-06	2.30E-07	9.09	2.66
Wafer[Lot]	4.00E-06	4.13E-07	36.36	4.78
Residual	6.00E-06	8.00E-06	54.55	92.57
Total	1.10E-05	8.64E-06	100.00	100.00

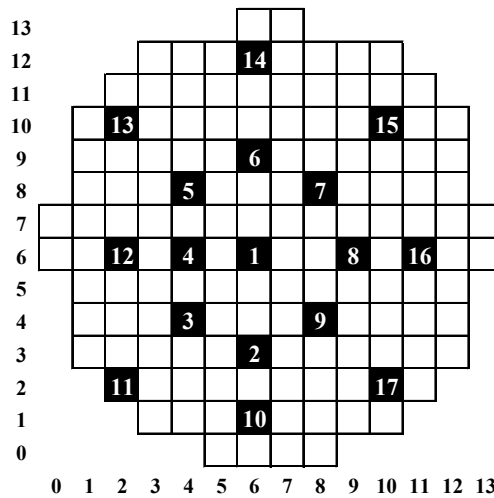


Figure 19. Pattern of exposure fields. Shaded fields were used for CD linewidth analysis.

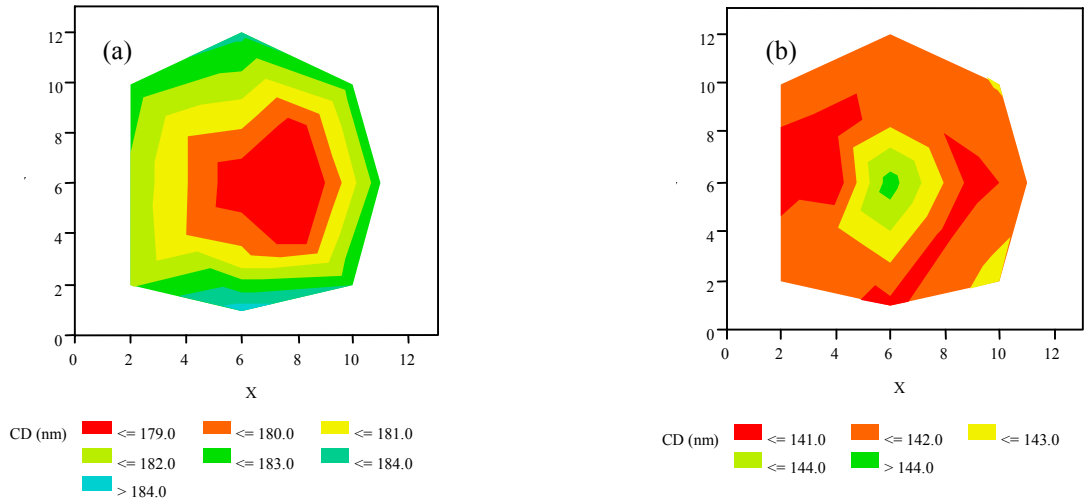


Figure 20. CD Contour map for 140 nm features using PEK-111A3; (a) isolated lines; (b) dense 1:1

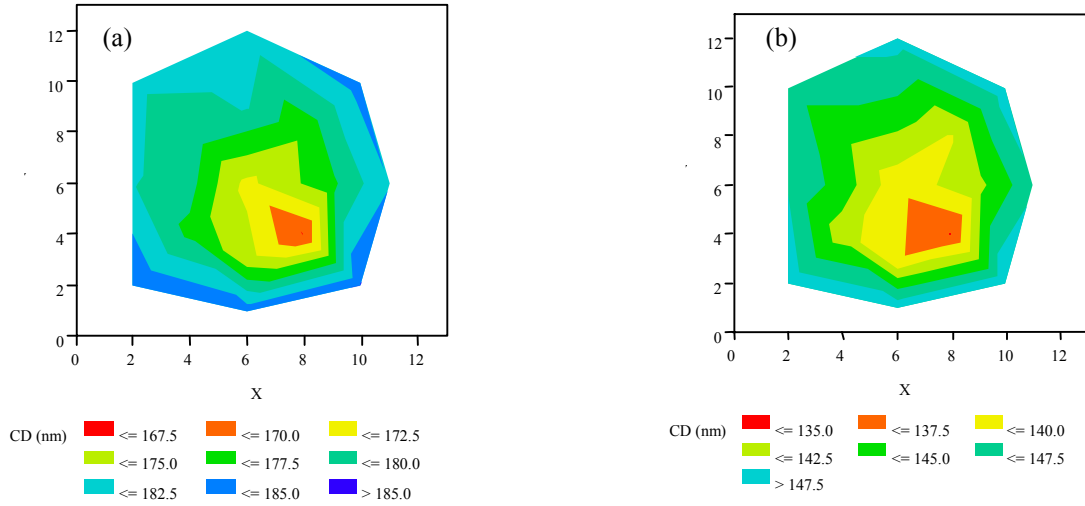


Figure 21. CD Contour map for 140 nm features using single PEB UV6 process; (a) isolated lines; dense 1:1 lines

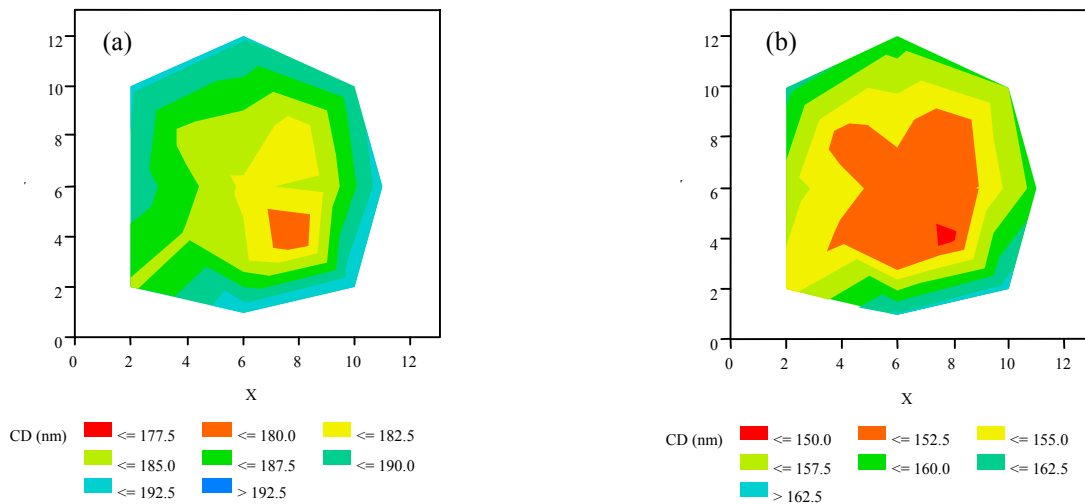


Figure 22. CD Contour map for 140 nm features using double PEB UV6 process; (a) isolated lines; dense 1:1 lines

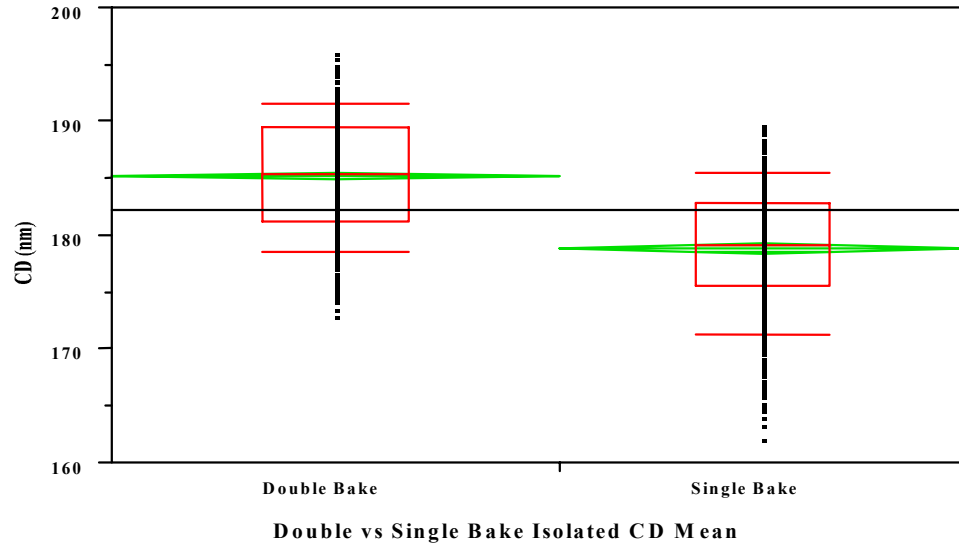


Figure 23. Box plot of mean CD values for 140 nm isolated lines.

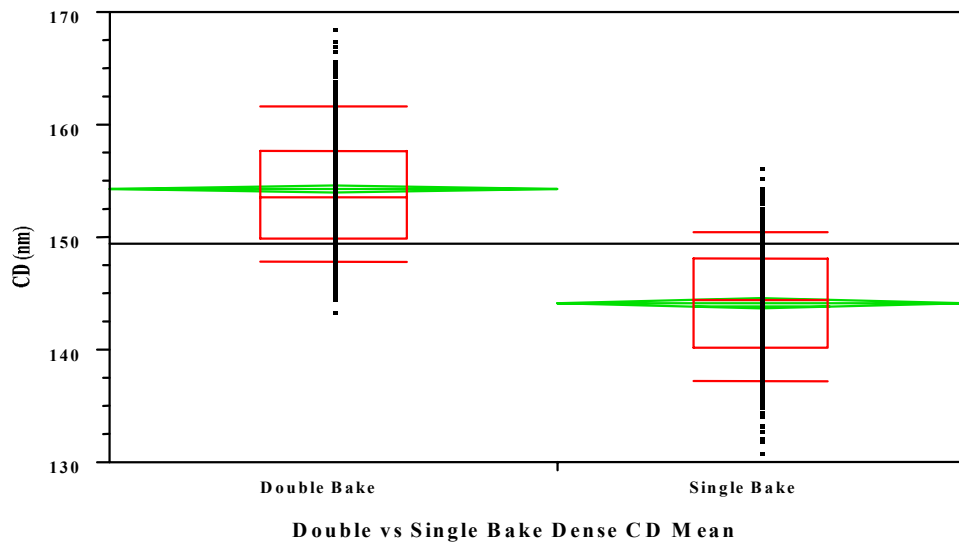


Figure 24. Box plot of mean CD values for 140 nm dense lines (duty cycle: 1:1).

Table 15. UV6 140 nm iso-dense line CD data analysis for double vs single PEB.

Process	Number		Mean		Std Dev		Std Err Mean	
	Iso	Dense	Iso	Dense	Iso	Dense	Iso	Dense
Double Bake	543	544	185.3	154.3	5.048	5.242	0.2167	0.2247
Single Bake	490	493	179	144.2	5.351	5.09	0.2417	0.2292

4. CONCLUSION

Processes capable of producing 160 and 140 nm dense lines with good CD control were developed for both a low E_A resist, PEK-111A3, and a high E_A resist, UV6. Unfortunately, a workable process involving low bias between grouped to isolated feature size was unattainable for either resist system. Moreover, limitations in the developed processes were shown to be related to poor phase uniformity in the mask and not associated with resist processes. Altering resist processes in an attempt to abate isolated to dense line size bias was unsuccessful for the low E_A and high E_A resist systems. Use of high E_A resist systems on 300 mm wafers may require more engineering than low E_A resist systems to eliminate marginal, systematic, across wafer CD size shift. Although the writing time and cost of the mask would increase, OPC is known to minimize iso-dense print bias. OPC features like scattering bar lines (sub-resolution features) effectively introduce an isofocal region to an isolated line so that the image through focus behaves like a dense line¹¹. The addition of OPC features to the altPSM mask used in these experiments is suggested as a method to decrease isolated to dense line size bias.

ACKNOWLEDGMENTS

The authors would like to thank Ronald Carpio, Jeffrey Byers, Al Stephen, Daniel Miller, Mike Pore, Don McCormack of SEMATECH, and Allan Awtrey of Tokyo Electron America, Inc. for their contributions. Our gratitude is also extended to Joe Johnson (Brewer Science), Peter Federlin (Sumitomo Chemical America, Inc.), and Wayne Ostrout (Shipley Company) for their donations and valuable discussions.

REFERENCES

1. G. Lee, "The Gain (And Pain) of 300 mm," *Future Fab* Vol. 1, Issue 5, pp. 61 – 63, Technology Publishing, London, 1998.
2. P. Burggraaf, "Optical lithography to 2000 and beyond," *Solid State Technology* Vol. 42, No. 2, pp. 31-41, 1999.
3. J. S. Petersen, M. McCallum, N. Kachwala, R. J. Socha, J. F. Chen, T. Laidig, B. W. Smith, R. Gordon, C. A. Mack, "Assessment of a Hypothetical Roadmap that Extends Optical Lithography Through the 70 nm Technology Node," *Proc. SPIE*, Vol. 3546, pp. 288-303, 1998.
4. M. D. Levenson, "The lithography crisis is now!," *Solid State Technology* Vol. 41, No. 6, pp. 288-87, 1998.
5. H. Liu, L. Karklin, Y. Wang, and Y. C. Pati, "The Application of Alternating Phase-shifting Mask to 140 nm Gate Patterning (II): Mask Design and Manufacturing Tolerances". *Optical Microlithography XI, Proc. SPIE*, Vol. 3334, 4, pp. 2-14, 1998.
6. R. D. Allen, W. E. Conley, R. R. Kunz, "Deep UV Resist Technology" Chapter 4 in *Handbook of Microlithography*, Ed. P. Rai-Choudhury, SPIE Optical Engineering Press, Bellingham, WA, 1997.
7. J. D. Byers, private communications.
8. J. S. Petersen, J. D. Byers, R. A. Carpio, "The Formation of Acid Diffusion Wells in Acid Catalyzed Photoresists" *Microelectronic Engineering* 35 pp. 169-174, 1997.
9. D. Miller, private communications.
10. J. L. Sturtevant, S. J. Holmes, P. Rabidoux, "Postexposure bake characteristics of a chemically amplified deep-ultraviolet resist" *SPIE*, Vol. 1672, pp. 114-124, 1992.
11. R. Gordon, C. Mack, J. Petersen, "Design and analysis of manufacturable alternating phase-shifting masks" *SPIE* Vol. 3546, pp. 606-616, 1998.